BUILDING A GIS FRAMEWORK FOR CO-ANALYSIS OF MINI-RF BISTATIC RADAR DATA WITH OTHER LUNAR DATASETS. J. M. Leeburn[1,2] , L. M. Jozwiak[2] , G. W. Patterson[2] , A. M. Stickle[2], and C. A. Nypaver[3] [1]Dept. of Earth and Mineral Sciences, Pennsylvania State University, University Park PA 16801, USA (jeff.leeburn@jhuapl.edu), [2]Johns Hopkins University Applied Physics Laboratory, Laurel MD 20723, USA, [3]Dept. of Earth and Planetary Sciences, University of Tennessee, Knoxville, TN.

Introduction: The NASA Lunar Reconnaissance Orbiter (LRO) has operated at the Moon for over 10 years, accumulating an unprecedented volume and variety of data characterizing the lunar surface. One such collection is that obtained by the Miniature Radio Frequency Experiment (Mini-RF). Mini-RF monostatic data have previously been semi-controlled or controlled to other datasets. Until recently however, registration errors have rendered Mini-RF bistatic data difficult to analyze with other lunar datasets. Here we present registered Mini-RF bistatic data in a GIS framework for the purpose of facilitating co-analysis with other lunar datasets.

Background: Mini-RF is a hybrid-polarized synthetic aperture radar (SAR) that operates at S-band (λ=12.6 cm) and X/C-Band (λ=4.2 cm) frequencies [1]. From launch of the LRO spacecraft in June of 2009 through to December of 2010, Mini-RF utilized a monostatic architecture (i.e., instrument antenna operates as the transmitter and receiver). In that time, Mini-RF collected data that covered > 66% of the lunar surface and > 95% of the lunar poles. Semi-controlled global mosaics of these data are available at the PDS [2] and controlled mosaics of these data for both poles have been produced by the USGS [3].

In May of 2012, Mini-RF transitioned to a bistatic architecture using the Arecibo Observatory (AO) and Goldstone deep space communications complex antenna DSS-13 as transmitters. To date, 33 S-band and 44 X-band bistatic observations have been collected of the lunar nearside and poles. These data are processed into radar images using a time-domain back-projection algorithm [4] that is sensitive to input topography.

An initial version of that algorithm formed radar images assuming a spherical Moon. While this choice did not affect overall data quality, it caused non-systematic errors in registration for each collect. This resulted in uniform pixel offsets, with the exact amount unique to each collect (Fig 1). Some collects also exhibited internal registration errors resulting in additional offset which varied across the length and width of the collect. Recent improvements to that algorithm [5] have allowed the incorporation of a low resolution topographic model of the lunar surface (LOLA LDEM4). Images produced since implementation of the new processing algorithm show marked improvement in topographic control but retain a fairly systematic along-track offset on the order of 2-3 km. In order to make this data usable in conjunction with other LRO datasets, we mitigate this offset, and smaller residual cross-track offsets (order of 100s of m), through georectification in a GIS framework.

Methodology: We created a database of georeferenced mosaics and shapefiles for commonly used LRO data products, which are readily manipulated by both commercial and open source geographical information systems (GIS). This data structure allows for both map-based and numerical queries, but also includes the analysis capability of GIS platforms such as spatial statistics, topographical applications, and raster calculations, among other quantitative operations.

Each Mini-RF collect is represented by eight separate images and a footprint shapefile. These mosaics contain values for the Stoke's products and CPR, as well as rasterized records of the phase, emission, and incidence angle for each collect. The footprint file indicates the spatial extent of each collect and contains metadata including orbit number, collection date, and wavelength to allow data searches based on these characteristics.

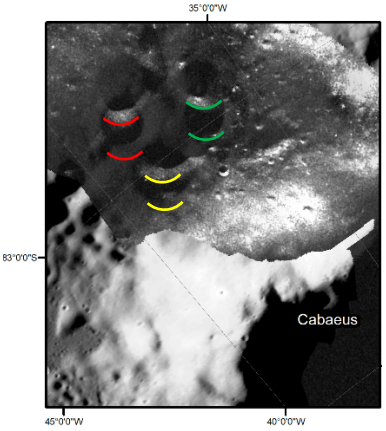

Figure 1: Example of linear offsets between S1 overlay and WAC imagery on Cabaeus southern rim. Arcs represent corresponding rims for each of the three unnamed craters indicated.

To remedy registration offsets, we performed affine transformations using three or fewer tie points to remove the uniform offset of each collect without warping individual pixels. These tie points where selected by a visual assessment of each S1 product and identification of regionally unique pixel groups, typically morphological features or crater rims (e.g. Fig 1). Corresponding pixel groups were then located on an LRO Wide Angle Camera (WAC) [6] 100m/pixel near-global basemap with projection supported by a 100m/pixel WAC-derived DEM (GLD100) [7]. From each group, a pair

of corresponding pixels was selected and the S1 pixel transposed to the location of the WAC pixel. For collects exhibiting nonlinear offsets, priority was given to minimizing error at the target of the collect.

Additional datasets: In order to promote co-analysis between instruments, we added several additional data products from other LRO instruments. Each was converted to the same projection and data format as the Mini-RF collects.

Lunar Orbiter Laser Altimeter (LOLA): Previous work has rectified existing LOLA laser-altimetry derived elevation measurements using stereo-derived terrain models to correct orbital and geolocation point errors [9]. The result is a 512m/pixel near-global digital elevation model (DEM) offering the highest lunar elevation accuracy currently available. We include a full global mosaic which has been projected to a geographic coordinate system, and reports normalized elevation in meters.

Diviner Radiometer: The Diviner 7-channel radiometer experiment has created several notable secondary datasets. We selected for inclusion the near global (±60 degrees) rock abundance map and regolith temperature maps [10]. In alignment with the goal of enhancing current research on polar volatile inventory and distribution in lunar remote sensing [11], we also include rasterized Diviner south pole average and seasonal maximum/minimum temperatures for the South pole region from -90 to -70 degrees. Permanently shaded regions (PSR) near the lunar poles have been recently confirmed as accumulation sites hosting water ice in part through the analysis of Diviner data [12], and we expect these Diviner and PSR datasets will experience heavy use as studies of such regions continue.

Future Work: We intend to make this data package available to the community for integrated studies, allowing more efficient exploration of lunar polar regions and benefitting ongoing studies in support of future missions. Figure 2 shows a simple representation of the integration already possible with the existing structure. Feedback from initial users will inform the inclusion of additional datasets deemed useful beyond these. This data package will provide an analysis-ready resource to lunar researchers, particularly those concerned with the distribution, extent, and quantity of lunar volatiles.

References: [1] Raney R. K. et al. (2011) *Proc. IEEE, 99*, 808–823. [2] Cahill, J.T. et al. (2014) *Icarus*, 243, 173-190. [3] Kirk R. L. et al. (2013) *LPSC XLIII,* Abstract #2920. [4] Patterson et al. (2017) *Icarus 283*, 2-19. [5] Turner, F.S. et al. (2019) *4th Plan. Data Work.,* Abstract #7075. [6] Robinson, M.R. et al. (2010) *Space Science Rev* 150, 81. [7] Robinson, M.R. et al. (2012) *Int. Arch. Photogramm. Remote Sens. Spat. Inf.* 39, B4. . [8] Barker, M.K. et al. (2016) *Icarus* 273, 346-355. [9] Bandfield, J.L. et al. (2011) *JGR Planets* 116 E12. [10] Li, S. et al. (2018) *PNAS* 115, 36. [11] Mandt, K.E. et al. (2016) *Icarus* 273, 15, 114-120.

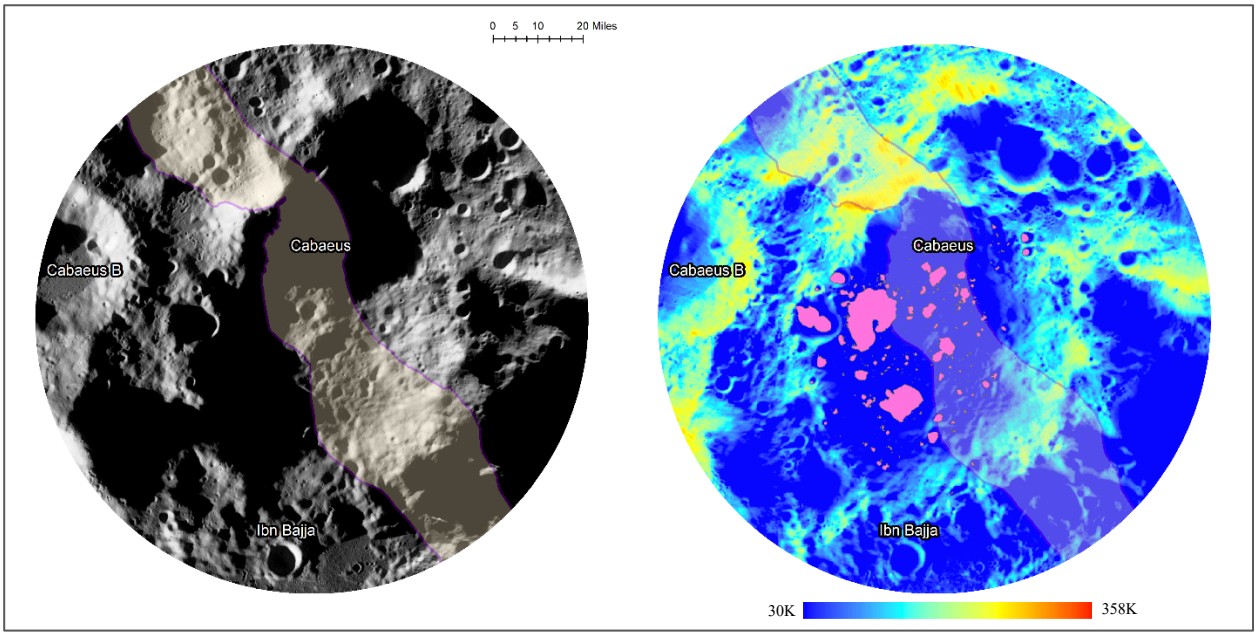

Figure 2: Illustrative example of footprint functionality depicting Mini-RF X-band bistatic coverage of Cabaeus crater near the lunar south pole over the 100m/pixel WAC mosaic (left) and rasterized Diviner average bolometric temperatures (right). Pink regions indicate known PSR locations. Such functionality allows easy assessment of data coverage and feasibility of target analysis. Scale bar is accurate for both figures, temperatures are in Kelvin.